DOI: 10.13009/EUCASS2019-129

Multidisciplinary Design of Reusable Re-Entry Vehicles by Optimization and Computational Fluid Dynamics

Andrea Aprovitola, Luigi Iuspa, Giuseppe Pezzella and Antonio Viviani
andrea.aprovitola@unicampania.it; luigi.iuspa@unicampania.it
giuseppe.pezzella@unicampania.it; antonio.viviani@unicampania.it
Department of Engineering, University of Campania "L. Vanvitelli". Aversa. Italy

Abstract

This paper deals with the development of a multi-fidelity design framework for reusable re-entry vehicles. A multidisciplinary shape optimization procedure, for Low Earth Orbit re-entry missions, is performed using a parametric model able to promote the search for unconventional concept aeroshapes. Low order fidelity methods are adopted in the optimization procedure to obtain several design candidates reasonably consistent with a set of mission requirements and constraints at an affordable computational time. Optimal design candidates are validated performing more reliable Computational Fluid Dynamics simulations in a set of specified waypoints along with the re-entry trajectory.

1. Introduction

Over the last decades, several private companies and Space Agencies worldwide developed space vehicle concepts with new re-entry technologies to perform Low Earth Orbit (LEO) missions. Current design requirements focus on vehicle reusability which implies a drastic cost reduction and determines short turnaround times to reconfigure a vehicle after a mission. With the Space Shuttle dismission, Reusable Launch Vehicle (RLV) programs focused on small scale demonstrators aimed at performing a controlled LEO re-entry, eventually landing with a braking parachute. European Space Agency program developed two demonstrators; the European eXperimental Vehicle principally aimed at recollecting data for future design activities, and the Intermediate eXperimental Vehicle (IXV) which performed a full-atmospheric re-entry at orbital speed [1]. A more mature configuration the X-37B, performed several missions, carrying small payload into orbit, and successfully landed on runway [2]. Additionally, two spaceplane projects the Dream Chaser (developed by Sierra Nevada Corporation), and the Space-Ship Two (by Virgin Galactic) are currently ongoing [3]. Those vehicles represent a further development of re-entry technologies and are expected to be capable of carrying crew to/and from LEO orbit. Several trade-offs (hypersonic vs subsonic aerodynamic efficiency, weight vs cross range, and size compatibility with fairings of launcher) which drive the overall design of aero-shapes are currently considered. Additionally, the emerging demand for space tourism also requires further constraints such as moderate g-load landings on a conventional runway.

An RLV concept achieves LEO orbit with an expendable/semi-reusable launcher; and eventually re-enters in Earth atmosphere either landing as a glider or alternatively using its own propulsion. During the re-entry phase RLVs experience very different flow/speed regimes characterized, among others, by high temperature real gas phenomena (i.e., thermo-chemical non-equilibrium flow, catalysis, viscous effects, and shock wave/boundary layer interaction). The above cited phenomena significantly affect vehicle performances and as well as different regions of its aeroshape during the early segment of re-entry trajectory, and represent the main design concern for the overall mission to be successful. A further consideration on vehicle design relates to the subsonic phase of re-entry. Indeed, blunt aeroshapes favor the hypersonic stage, but the resulting vehicle aerodynamic efficiency at subsonic speed is penalized. Therefore, a single aeroshape does not fit all design requirements, and performances of a re-entry shape can only be improved considering a complex trade-off between several objectives.

With this in mind, the Multi-disciplinary Design Optimization (MDO) became the only viable option routinely adopted in the conceptual design phase of a re-entry vehicle since the large number of design variables result in conflicting trends [4]. Indeed, a multi-disciplinary analysis involves numerous disciplines such as geometry creation, aerodynamic computations, trajectory estimation, and thermal analysis.

In this framework, Non-Uniform Rational B-spline (NURBS) parameterization has become the standard tool used for complex aero-shape design because of their useful geometrical properties, thus allowing an efficient sampling of search space of design parameters [5]. NURBS increase the local control of the vehicle aeroshape and handle complex modeling tasks such as wing-fuselage junctions, winglets and vertical fins (i.e., NURBS patches). Multidisciplinary

DOI: 10.13009/EUCASS2019-129

analysis requires that disciplines are fed according to the input data computed by the previous discipline and eventually design data are processed to the optimization algorithm.
Owing to complexity of the problem, in MDO are used engineering tools based on several simplifying assumptions. Those methods allow handling the complexity of the problem with a low computational overhead, however resulting accuracy is penalized. Therefore, more reliable tools must be adopted to validate a single trade-off configuration.
In this framework, the present research effort deals with the development of a multi-fidelity design procedure for a reusable unmanned re-entry vehicle, able to perform a safe and reliable LEO de-orbit descent, ending with an horizontal landing on a conventional runway. The computational framework integrates a multidisciplinary optimization to obtain a range of aeroshape variations that are reasonably consistent with all the constraints of flow regimes encountered during re-entry flight, while satisfying mission requirements.
Finally, as discussed in the paper, design reliability of optimal candidates is also addressed by performing more accurate Computational Fluid Dynamics (CFD) simulations for a set of specified waypoints along with the re-entry trajectory, according to a trajectory-based design approach.

2. Rationale

The present research study combines two computational procedures, with different level of fidelity to perform and validate the conceptual design of an innovative hypersonic glider, namely aerodynamic panel methods (PM) and CFD [6]. The former (i.e., PM) belongs to the engineering-based tools, referred to as Low Order of Fidelity (LOF) methods [7]. The latter (i.e., CFD) is a numerical-based tool of High Order of Fidelity (HOF) methods [7]. It allows simulating the whole flowfield that takes place past the vehicle concepts. LOF tools are embodied in an in-house developed design framework, which supports an MDO procedure for a LEO re-entry mission with maximum cross-range flight and finalized with a conventional runway landing maneuver. LOF methods are suitably adopted in multidiscipline analysis because of their low computational overhead. Indeed, they allow sub-discipline computations at each iteration of the optimization. Therefore, a robust genetic algorithm capable to handle global design objectives is adopted.
The MDO procedure individuates several design candidates, which represent feasible instances of a re-entry configuration. Several mission constraints (i.e., thermal and dynamical) ensuring a safe re-entry corridor, are assigned and define the boundaries of the search space. The reliability of optimization results of the selected design candidate are then addressed by comparing concept's engineering-based aerodynamics to that suggested by performing HOF-CFD computations for a representative range of flight conditions. Because the peculiar design parameterization promotes the search for unconventional innovative concept's configurations, and HOF-CFD simulations account for several fluid dynamic phenomena that are not addressed by LOF solvers, HOF data are also used to validate aerodynamic computations performed with LOF.

3. Multidisciplinary Design Optimization

3.1 Re-entry flight scenario and multidisciplinary analysis

The MDO procedure assumes a re-entry corridor defined according to a given number of flight conditions, namely waypoints, shown in Table 1. Waypoints (1-4) are only a rough approximation of an unpowered gliding re-entry from a LEO orbit, see Figure 1.

Table 1: Selected trajectory waypoints for MDO procedure.

	Altitude, (Km)	**Mach No, (-)**	**AoA, (deg)**
Waypoint (1)	$40 < z \leq 120$	$M_\infty \leq 23$	$35° - 50°$
Waypoint (2)	$20 < z \leq 40$	$M_\infty \leq 3.6$	19°
Waypoint (3)	$10 < z \leq 20$	$M_\infty \leq 2$	14°
Waypoint (4)	$z \leq 10$	$M_\infty \leq 0.3$	10°

DOI: 10.13009/EUCASS2019-129

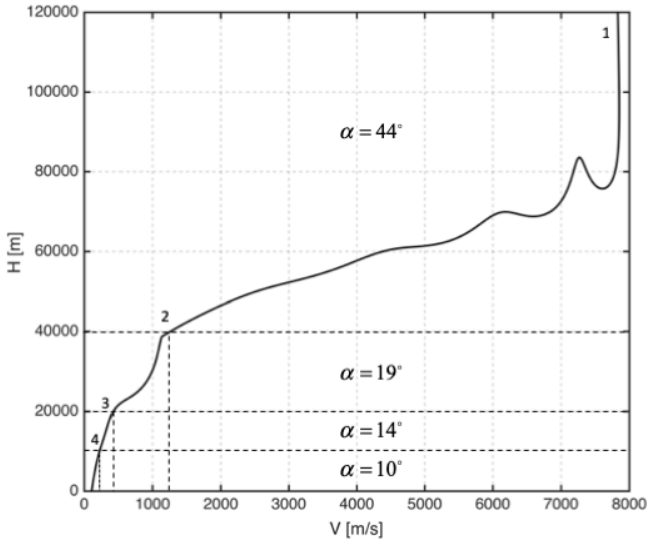

Figure 1: Reference re-entry trajectory chosen for the optimization.

However, they represent a re-entry flight envelope with a reasonable accuracy for a conceptual design study. A constant bank angle (μ_a) is assigned at waypoints (1-3) to ensure a cross range performance. Moreover, value of μ_a is set equal to zero at waypoint four to simulate a horizontal landing condition. The MDO procedure is formulated identifying each sub-discipline involved in the design process. Figure 2 specifies the input and output design variable adopted for each sub discipline and shows existing relation among them.

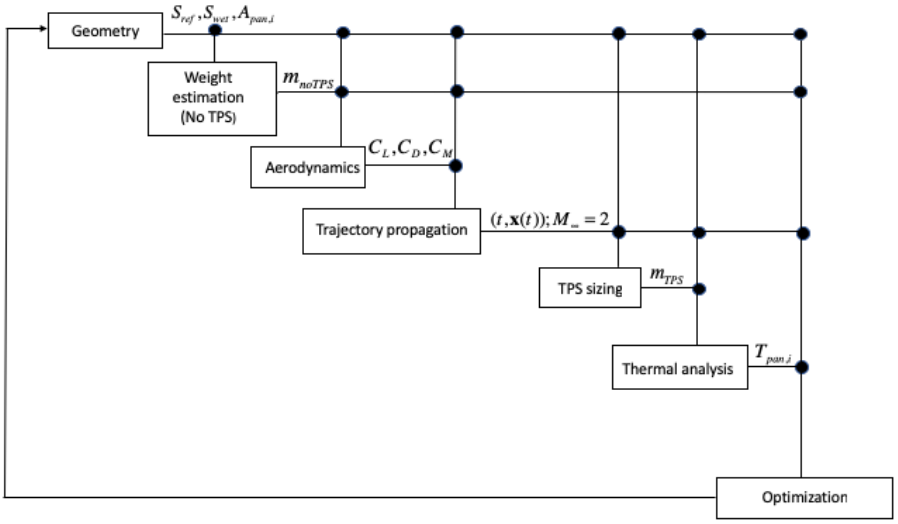

Figure 2: Sub-disciplines concurring in MDO.

Each sub-discipline analysis is performed independently and provides the input parameters for the next analysis. Sub-discipline models are finally connected to an optimization algorithm. A proprietary geometry module gives a support for several engineering-level methods which comprises: i) a multi-regime aerodynamic analysis (i.e., Hypersonic/Supersonic/Subsonic flow) performed with PM flow solvers; ii) a three degree of freedom non-planar trajectory estimation; ii) a trajectory-based aeroheating analysis for Thermal Protection System (TPS) sizing; iv) a mass estimation procedure.

3.2 Geometry module

Geometry module implements a proprietary parametric procedure, that has been fully detailed in Ref. [8]. Lifting body or winged re-entry vehicles are created as monolithic bodies differently from conventional techniques based on

DOI: 10.13009/EUCASS2019-129

explicit use of several NURBS surface parameterizations. A wireframe, shown in Figure 3-a encloses a box-shaped volume with assigned dimensions, and defines the geometric support for a surface grid.
Shape variations are precisely accounted using cubic rational B-splines, and piece-wise linear interpolators adopted in the cross-sectional plane, and in the wing-plane of the wireframe. Vehicle shapes are eventually represented as a computational grid (see Figure 3-c) with points obtained by a linear interpolation on a set of sampled point on wireframe (see Figure 3-b).
Finally, vehicle shape is represented as a structured mesh composed of quadrangular flat panels.

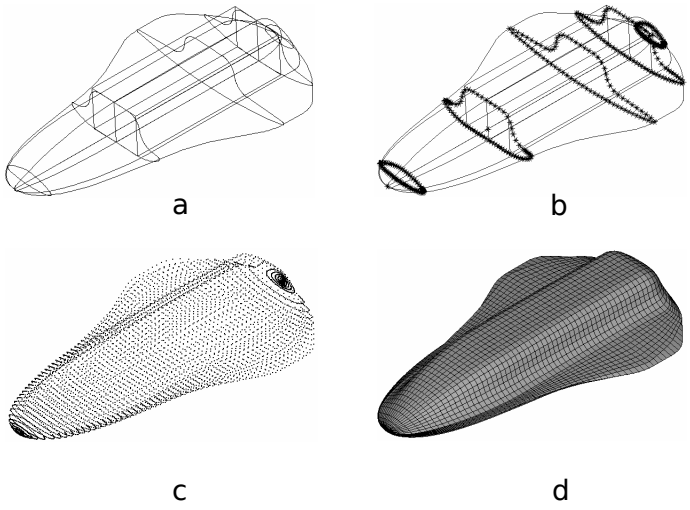

Figure 3: (a) wireframe definition; (b) uniformly sampled points on some specified cross sections; (c) linear interpolation of points; (d) surface panel mesh.

The proposed methodology creates geometries that are homeomorphic with respect to a spherical surface without singularities. Therefore, shape instances returned by a search space sampling are topologically invariant. As a direct consequence of this property, the discretized surface shape can be assumed to be mapped in UV coordinates over an equivalent cylindrical surface.

An equivalent mesh arrangement by using a more conventional technique based on explicit NURBS support geometries, cause a possible fragmentation of patches with a parameter-dependent variable topology.

3.3 Aerodynamics

Aerodynamic module implemented in MDO computes aerodynamic force and moment coefficients according to flight conditions of Table 1 as functions of Mach, Altitude and concept attitude (M_∞, h_∞, α). Frictionless coefficients are obtained with publicly available panel solvers (hypersonic or potential) built in the computational procedure, and suitably selected by the value assumed by the AoA. As shown in Figure 4, the vehicle surface has been approximated by using a structured mesh composed of Np =6282 quadrilateral panels with an edge length of 120 mm. The current resolution provides the mesh-independence of the aerodynamic coefficients respect to the upper and lower bounds of the geometric design parameters. Hypersonic Surface Impact Methods (SIM) are adopted to compute aerodynamic coefficients up to M=2. SIM methods determine the pressure distribution over a three-dimensional body, at hypersonic Mach numbers, solely considering the local impact angle between the free-stream flow and the body. Generally, trade-offs evaluations between different SIM methods are routinely performed to find the most appropriate method for a generic shape instance.

DOI: 10.13009/EUCASS2019-129

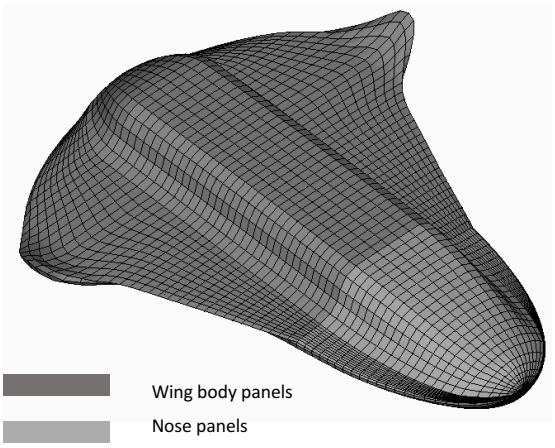

Figure 4: Panel mesh adopted for Aerodynamic computations.

A general criterion suggests the use of Newtonian or Modified Newtonian methods, for impact flow regions (assimilated as a spherical surfaces) on the nose either placed on windward or leeward side. Tangent cone method can be suitably applied to blended wing-body sections.
In the present computations, panel surface is partitioned in two sub-groups as shown in Figure 4, and panel methods chosen for each sub-group are reported in Table 2.

Table 2: SIM Methods adopted for Hypersonic Aerodynamics.

	Panel sub-group	**Windward**	**Leeward**
SIM-I	Nose	Modified Newtonian	Prandtl-Meyer
SIM-I	Nose	Tangent Cone	Prandtl-Meyer

Finally, aerodynamic coefficients of the vehicle at incompressible Mach number, are computed by adopting the integral formulation of potential generated by a distribution of singularities (sources and doublets), using the opensource tool [9].

3.4 Mass estimation

The TPS is designed with two of the materials adopted for the Space Shuttle thermal insulation system, namely the Reinforced Carbon-Carbon Composite (RCC) and the High-Temperature Reusable Surface Insulation (HRSI) made of coated LI-900 Silica ceramics. RCC material is used only for insulation from the peak wall temperatures (i.e., nose and wing leading edges and concept belly side), while the LI-900 material is used for the remaining vehicle surface. The heatshield thickness all around every cross-section is distributed according a bi-linear law, and the nose thickness is used as design variable. A mass decoupling model, based on the set of relations reported in Ref. [8], is considered.

3.5 Flight mechanics and Aero-heating analysis

Re-entry trajectory is computed in a non-rotating, inertial, Earth-Fixed Earth-Centered (ECEF) frame of reference. The vehicle is assumed as a point mass, describing a non-planar re-entry trajectory with a bank constant angle μ_a that is also assumed as a design variable of the optimization. Furthermore, the vehicle dynamics is described by a four degrees of freedom point mass model, provided the implicitly defined modulation law of the AoA reported in Table 1. An unpowered re-entry maneuver from an altitude $h(t_0) = 120$ km and speed $V(t_0) = 7835$ ms^{-1} is considered

DOI: 10.13009/EUCASS2019-129

assuming values of longitude θ, latitude ϕ, and flight azimuth χ all set to zero. A conventional landing is simulated assuming at waypoint four $\mu_a = 0$ and a maximum touch-down velocity $V_{td} \leq 110 m/s$.
The thermal state of the TPS is determined considering the kinematic trajectory data up to $M = 2$, significant for thermal heating. TPS exterior (w_2) and interior (w_1) wall temperatures are computed to determine the choice and size of the coating material. TPS surface is discretized using the panel mesh previously defined for aerodynamic analysis; a one-dimensional model of TPS thickness is adopted with computational nodes i defined at centroids of the panel mesh.

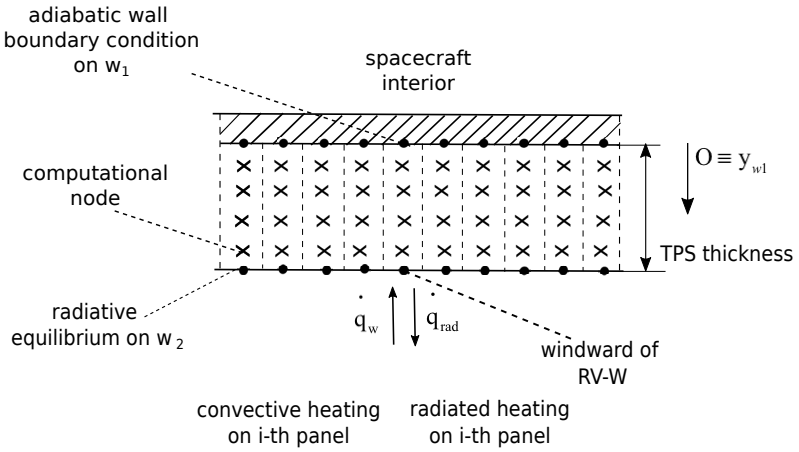

Figure 5: Panel mesh adopted for Aerodynamic computations.

The thermal analysis is only performed on windward side being the maximum heated region of TPS; the leeward side of the vehicle is supposed to be at fixed wall temperature.
Radiative equilibrium assumption ($\dot{q}_{w_2} = \dot{q}_{rad} = \sigma \varepsilon T_{w_2}^4$) allows to compute the exterior wall temperature $T_{w2,i}$ which represents a boundary condition for heat-conduction problem. The interior TPS wall temperature T_{w1i} is computed at each node of the discrete $i-th$ panel of the TPS mesh, using a one-dimensional unsteady heat-diffusion model. An adiabatic wall boundary condition is adopted on the interior wall of TPS, and the two TPS walls are considered initially at same temperature

3.6 MDO computations

The multidisciplinary analysis, summarized in the previous sections, supports a multi-objective optimization problem which aims to find the best candidate for the re-entry mission addressed in Sec. 3.1 in terms of minimum mass, and maximum cross range performances. Cross-range performances essentially depends on vehicle efficiency, while mass is influenced by the sizing and materials of TPS. Therefore, the selected objectives determine the overall design of shape both in high- and in low-speed regimes. The optimization constraints are formulated accounting the feasible temperature for the TPS materials $T_{w2} \leq \left(T_{\max,w_2}\right)_{RCC} = 1920K$, $T_{w1} \leq \left(T_{\max,w_2}\right)_{Li-900} = 1644K$, the maximum landing velocity $V_{td} \leq 110 m/s$, the load factor $n_z \leq 2.5$, and dynamic pressure $q_{dyn} \leq 14 kPa$ respectively. A number of $l = 29$ design variables x_i (geometric and aerodynamic) defines the state vector $\mathbf{x}$ of the optimization; the complete list of design parameters and their range of variation are reported in Ref. [8]. In Table 3 are shown the converged value of the most significant design parameters which influence hypersonic and subsonic performance of the vehicle length of the fore-overhang, nose radius and winglet bending angle.

DOI: 10.13009/EUCASS2019-129

Table 3: Design parameters at converged optimization.

	$l[m]$ **Total length**	$R_N[m]$ **Nose radius**	θ_w[deg] **bent angle**	$w_s[m]$ **wingspan**
Configuration(A)	8,150	0,379	0.9	8,2
Configuration (B)	9,252	0,469	40	8,6
Configuration (C)	9,212	0,446	13	8,5
Configuration (D)	10,122	0,598	37	9

Figure 6 (dashed line) shows the set of non-dominated solutions on Pareto front for mass and cross range objective and highlights the existing trade-off among them.

Four non-dominated design points (A)-(C) belonging to the Pareto's front are selected and highlighted. Among the selected configurations design (B) depicts a reasonable trade-off between the objective functions. Therefore, we selected configuration (B) for the comparison with HOF methods.

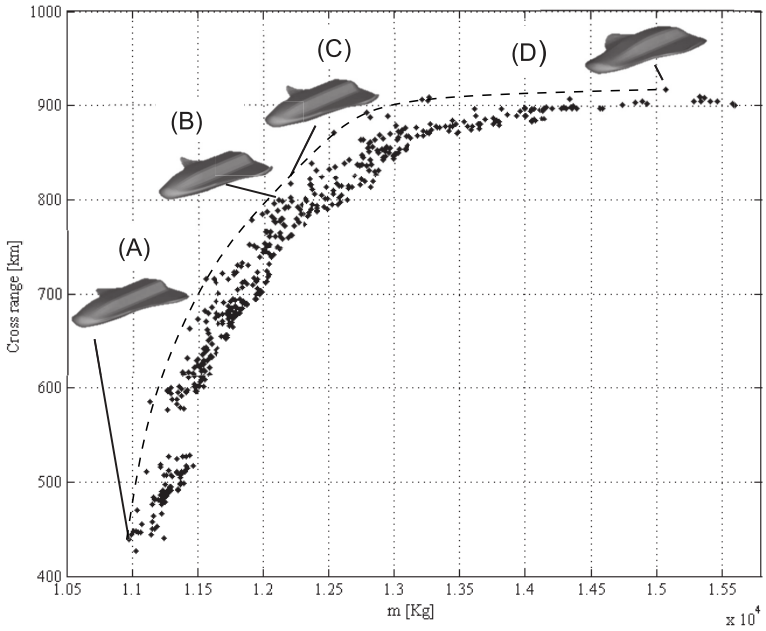

Figure 6: Design candidates on Pareto front: (A) Minimum mass; (B) trade-off configuration; (C) medial design candidate; (D) maximum cross-range.

4. Results

A three-view drawing of configuration (B) is shown in Figure 7. The overall dimensions are summarized as follows: length $l = 9252$ mm; height $h = 1500$ mm; wingspan $w_s = 8600$ mm; nose radius $R_n = 469$ mm; bent angle $\theta = 40^\circ$; total mass $m = 12105$ kg Configuration (B) features a monolithic blended wing-body with a double-delta wing planform which is beneficial for thermal loads reduction at wing leading edge.

DOI: 10.13009/EUCASS2019-129

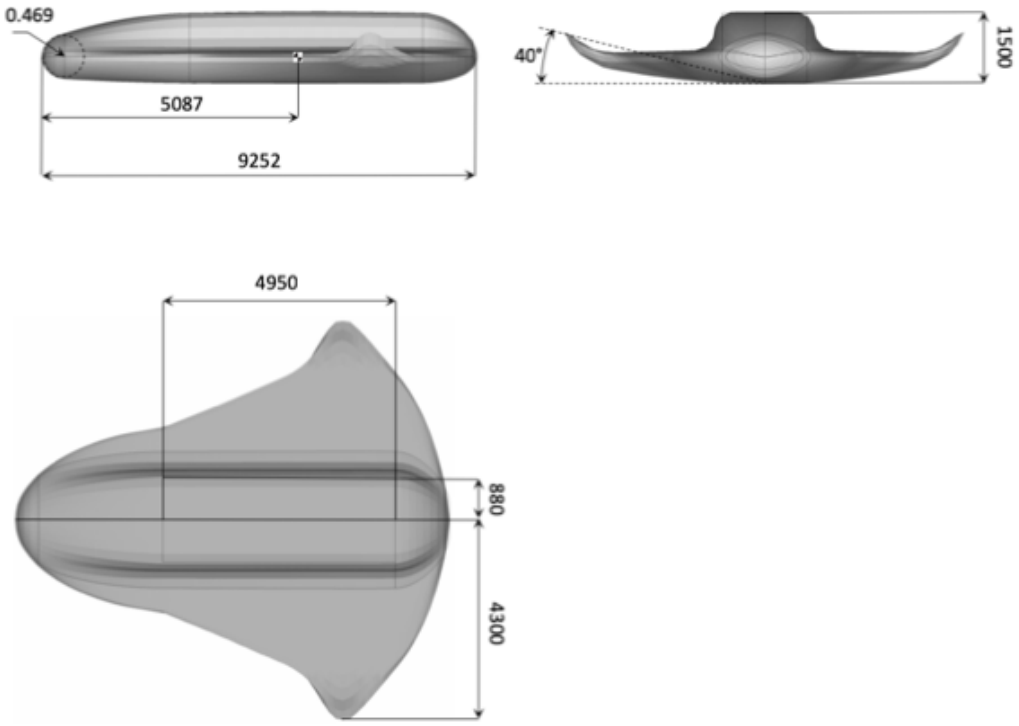

Figure 7: Three-view of selected (B) trade-off configuration adopted for aerodynamic computations.

Furthermore, a flat bottom surface and a blunted nose provides a significant increase of hypersonic performance.

Table 4: SIM Method adopted for LOF-HOF aerodynamic comparison.

	Panel sub-group	**Windward**	**Leeward**
SIM-I	Nose	Modified Newtonian	Prandtl-Meyer
SIM-I	Wing/body	Tangent Cone	Prandtl-Meyer
SIM-II	Nose	Modified Newtonian	Prandtl-Meyer
SIM-II	Wing/body	Tangent Wedge	Prandtl-Meyer

The aerodynamic coefficients i.e. lift, drag, and moment coefficient are computed as follows:

$$C_i = \frac{F_i}{q_\infty S_{ref}}, \quad i = L, D$$

$$C_{my} = \frac{M}{q_\infty l_{ref} S_{ref}}$$

DOI: 10.13009/EUCASS2019-129

with: $S_{ref} = 44{,}6 \cdot 10^6\, mm^2, l_{ref} = 6220 mm$. Aerodynamic computations are performed with SIM methods as addressed in Sec. 3.3 considering the following range of angle of attack and Mach numbers: $M_\infty = 23{,}10{,}2; \quad \alpha = (-5, 10, 15, 20, 25, 30, 35, 40, 45, 50)$ [deg] respectively computed at $z = (120,\ 51.15, 0.680)$ [km]. Two different SIM methods are adopted on wing/body panel sub-group (see Figure 4) on the windward side namely tangent cone and tangent wedge, while for Nose panel sub-group Modified Newtonian method is adopted in both cases.

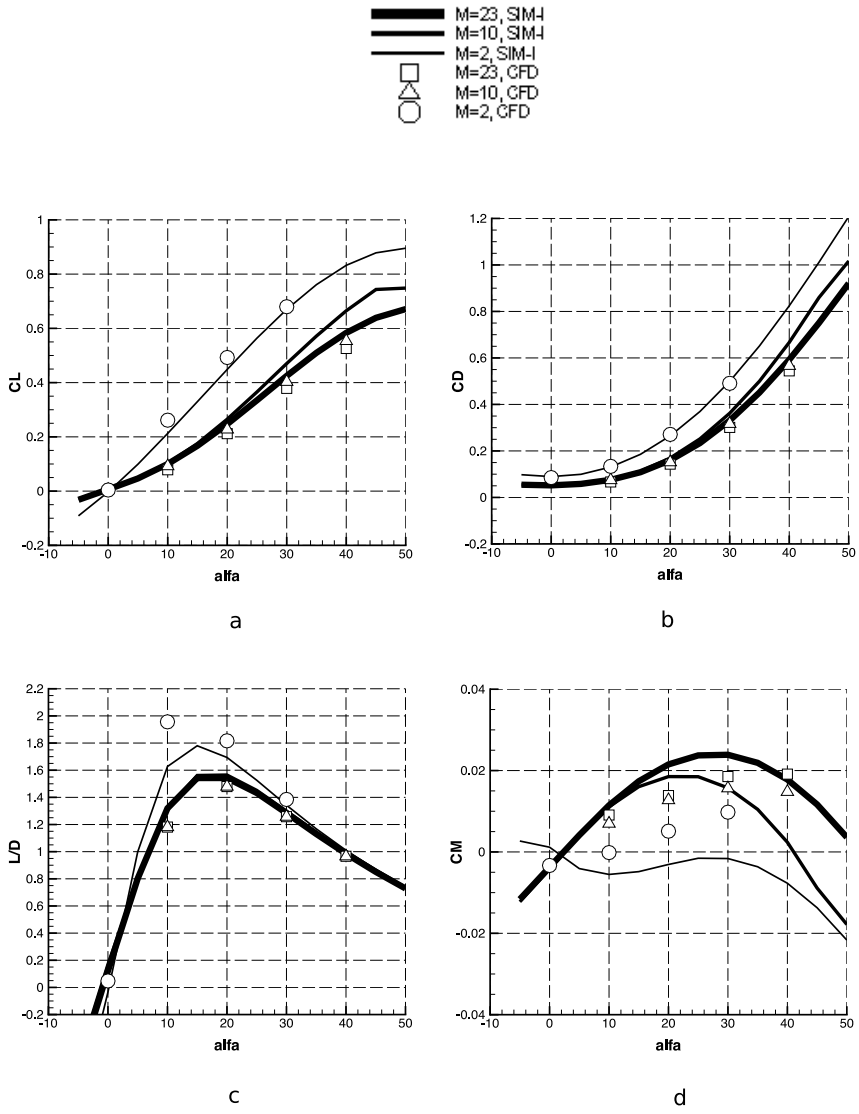

Figure 8: Comparison between Aerodynamic computations performed using SIM-I and Eulerian CFD computations: (a) Lift coefficient; (b) Drag coefficient; (c) aerodynamic efficiency; (d) pitching moment coefficient wrt CoG.

The geometric model guarantees shapes that are topologically invariant without adoption specific templates of shapes. Therefore, we cross-checked the results obtained using methods of group "SIM-I", with methods of group "SIM-II" to address a sensitivity analysis of aerodynamic coefficients to the local impact flow geometry. Figure 8a-d shows a comparison between aerodynamic computation performed with PMs (SIM-I) and Eulerian CFD computations at some specified AoA. Viscous effects are not considered in a preliminary aerodynamic estimation which is valid in conceptual design. As one can see, a rather good agreement with CFD methods is obtained both at low- and high-speed regimes as appears comparing lift and drag coefficient.

It is worth noting that agreement between CFD and panel methods is significant also at $M_\infty = 2$ at low incidence, where Newtonian theory departs from the main assumption of a thin shock layer. This result seems to suggest that the aero-shape shape even at relatively low incidence, creates obliques shocks which are very close to the solid wall,

DOI: 10.13009/EUCASS2019-129

similarly, to what happens at hypersonic Mach numbers. Figure 9a-b shows pressure contours superposed to iso-Mach contours where shocks are observed near winglet and nose. The oblique shocks which form over the winglets are responsible of the complex patterns of the stream-trace reported in Figure 9. As Eulerian simulation is concerned, the viscous separation is not properly represented (numerical diffusion mimics a sort of artificial viscosity, however its order of magnitude is far lower than laminar or turbulent viscosity). Flow streamtraces exhibit a three-dimensionality of velocity field represented by two vertical structures departing from the trailing edge of the winglets.
Furthermore, Figure9a also confirms the low local flow incidence between wing-body region which justifies the good agreement between LOF and HOF computations.

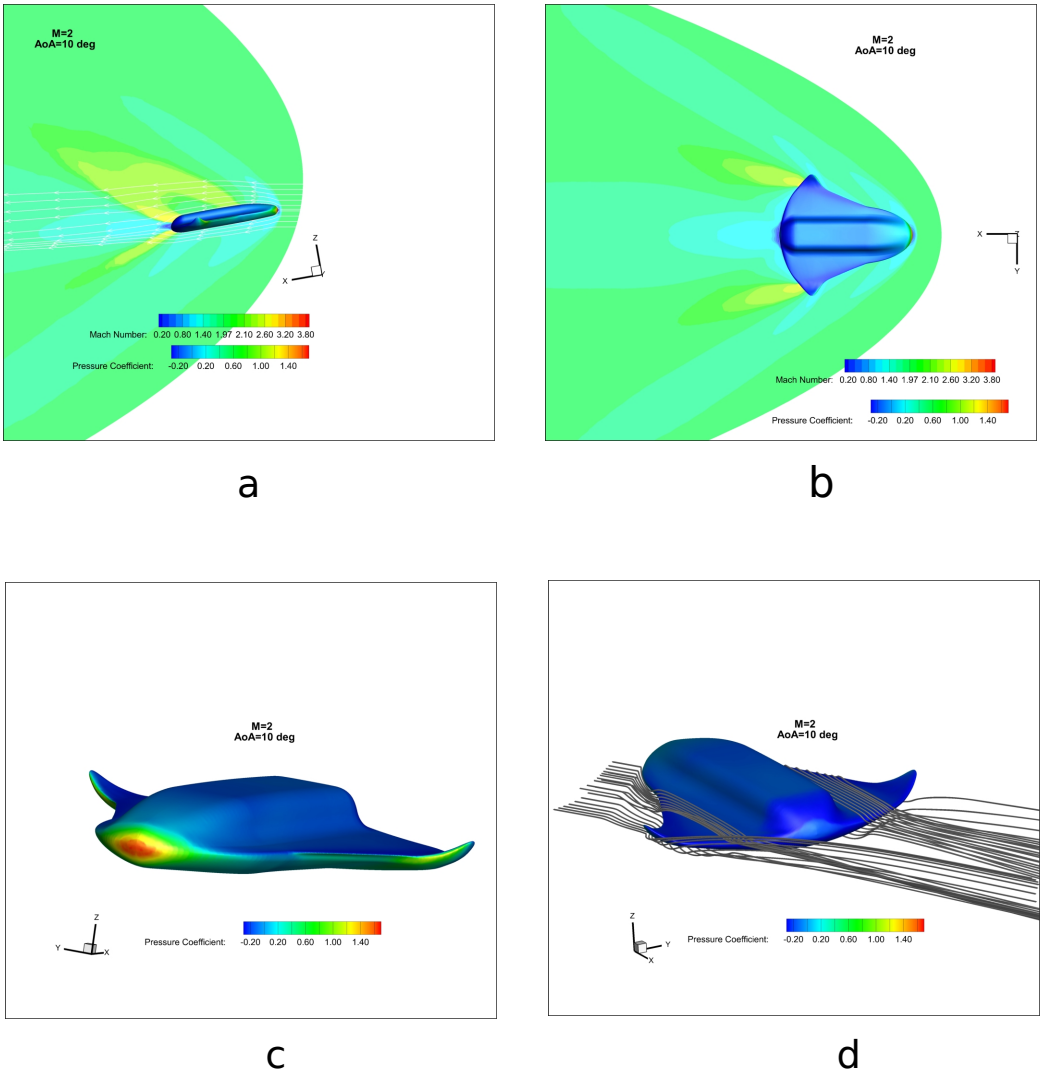

Figure 9: (a-c) Pressure coefficient at $M_\infty = 2$ and $\alpha = 10^\circ$; (d) stream-traces visualization.

The longitudinal pitching moment coefficient reported in Figure 8 is computed assuming the position of centre of gravity (CoG) at $X_{cg} = 55$ % of the longitudinal length. The comparison is not quite satisfying. However, this trend is due to the dimensions of the mesh panel which is of the order of static margin used for momentum computation.

DOI: 10.13009/EUCASS2019-129

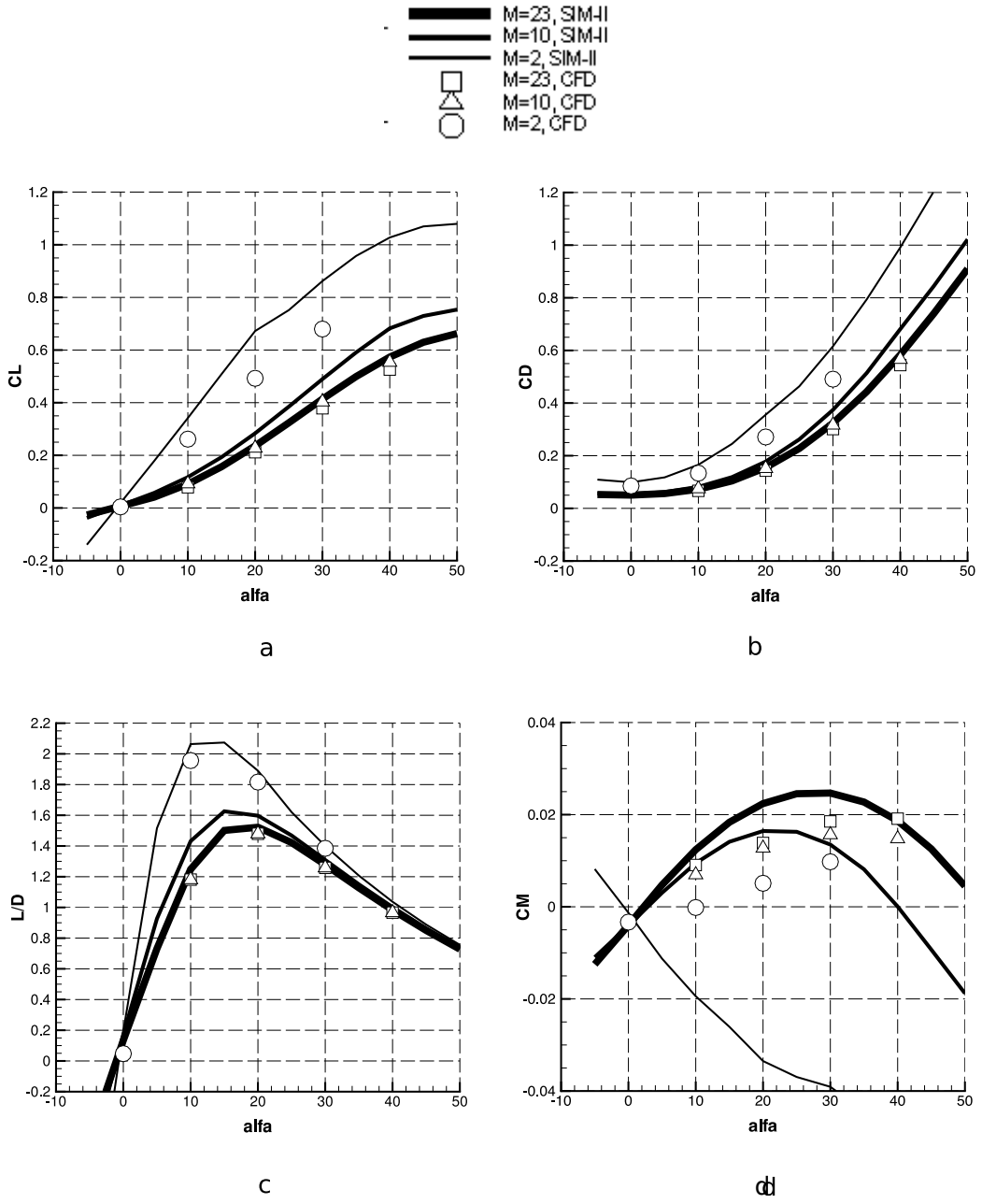

Figure 10: Comparison between Aerodynamic computations performed using SIM-II and Eulerian CFD computations: (a) Lift coefficient; (b) Drag coefficient; (c) aerodynamic efficiency; (d) pitching moment coefficient.

In Figure 10 are shown comparison between aerodynamic computation performed with methods of group “SIM-II” (see Table 4) and Eulerian CFD computation. Looking at Figures 8 and 10 it appears that Tangent Cone methods performs better than Tangent Wedge method at supersonic Mach number, while hypersonic computations are not significantly affected by the choice of SIM method on wing-body panel subgroup. The above observation confirms that the flow-field on the considered regions of vehicle surface cannot be assumed as two-dimensional as confirmed looking at stream-trace of Fig.9d.

DOI: 10.13009/EUCASS2019-129

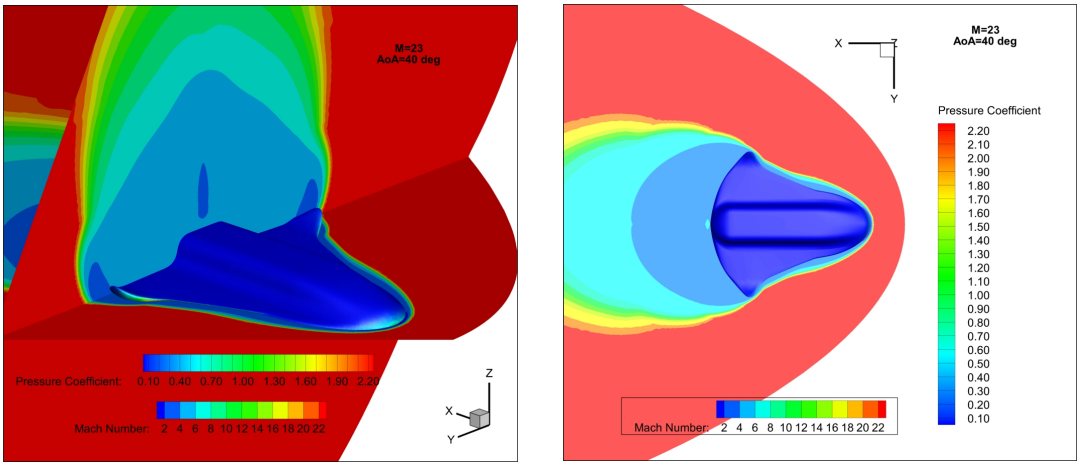

a b

Figure 11: Figure 9: (a-b) Pressure coefficient at $M_\infty = 23$ and $\alpha = 40^\circ$.

Finally, Fig.11a-b shows the pressure distribution at re-entry Mach number at AoA near to the optimal value $\alpha_{ott} = 44^\circ$. The aeroshape features a typical flow-field configuration during re-entry, where the nose blutness and the high AoA creates a detached bow shock, thus allowing both aerodynamic braking due to the wave drag and thermal dissipation to the surrounding flow.

5. Conclusions

In this work a design framework applied conceptual aero-shape design was developed. Computational tools with different level of fidelity were adopted and characterized the aero-shape design. It is found that the multidisciplinary optimization procedure, performed with low order of fidelity methods creates re-entry shapes with geometric features that are reasonably consistent with a multi-regime aerodynamics, and with the selected set of constraints. This evidence was confirmed by more reliable computational fluid dynamic simulations, that highlighted a good agreement relative to the main aerodynamic features of re-entry flow-field.

References

[1] Tumino, G. and Yves G., "ESA Bulletin 128 - IXV: the Intermediate eXperimental Vehicle." ESA, November 2006.
[2] A. Chaudhary, V. Nguyen, H. Tran, D. Poladian, E. Falangas, “Dynamics and Stability and Control Characteristics of the X-37”. AIAA-2001-4383.
[3] Howard, Russell D., Zachary C. Krevor, et al. “Dream Chaser Commercial Crewed Spacecraft Overview.” Proc. of 17th AIAA International Space Planes and Hypersonic Systems and Technology Conference, San Francisco, CA. 2011.
[4] D. Dominic And M. Erwin. Optimization of Entry-Vehicle Shapes During Conceptual Design. Acta Astronaut., 2014.
[5] B. Kulfan, J. Bussoletti. “Fundamental Parameteric Geometry Representations for Aircraft Component Shapes”. Multidisciplinary Analysis Optimization Conferences. American Institute of Aeronautics and Astronautics, September 2006. Doi: 10.2514/6.2006-6948. URL Http://Dx.Doi.Org/10.2514/6.2006-6948.
[6] Sziroczak, D., Smith, A review of design issues specific to hypersonic flight vehicles. Progress in Aerospace Sciences, 84:1–28 (2016).
[7] Hirschel, E., Weiland, C. Selected Aero-thermodynamic Design Problem of Hypersonic Flight Vehicles. Springer-Verlag/AIAA (2009).

DOI: 10.13009/EUCASS2019-129

[8] Viviani, A., Iuspa, L., Aprovitola, A. An optimization-based procedure for self-generation of Re-entry vehicle shape. Aerospace Science and Technology, 68: 123-134, (2017).
[9] D., Filkovic. APAME 3D panel method, www.3dpanelmethod.com.